Available online at www.sciencedirect.com
ScienceDirect
Quaternary International 169–170 (2007) 154–165

Paleoclimatic implications of oxygen isotopic variation in late Pleistocene and Holocene tusks of *Mammuthus primigenius* from northern Eurasia

David L. Fox[a,*], Daniel C. Fisher[b], Sergey Vartanyan[c], Alexei N. Tikhonov[d], Dick Mol[e], Bernard Buigues[f]

[a]*Department of Geology and Geophysics, University of Minnesota, 310 Pillsbury Dr SE, Minneapolis, MN 55455, USA*
[b]*Museum of Paleontology and Department of Geological Sciences, University of Michigan, Ann Arbor, MI 48109, USA*
[c]*Wrangel Island State Reserve, Pevek, 686870, Chukotka, Russian Federation*
[d]*Zoological Institute, Russian Academy of Sciences, Saint Petersburg 199034, Russian Federation*
[e]*CERPOLEX/Mammuthus, Hoofddorp, The Netherlands*
[f]*CERPOLEX/Mammuthus, Saint Mandè, France*

Available online 13 November 2006

Abstract

To understand the role of climate change in the extinction of *Mammuthus primigenius* in Eurasia, we examine spatial and temporal variations in growth increment and oxygen isotope ($\delta^{18}O$) profiles of radiocarbon dated mammoth tusks. We serially sampled tusk dentin in late Pleistocene tusks from the Taimyr Peninsula and Chukotka and Holocene tusks from Wrangel Island for a total of 241 oxygen isotope analyses from 11 tusks. Most sample series spanned 2–3 years of tusk growth. Differences in mean $\delta^{18}O$ values among the Taimyr tusks correlate with $\delta^{18}O$ values in corresponding intervals in the Greenland ice sheet and with regional paleoclimate reconstructions. The longitudinal gradient in $\delta^{18}O$ values of late Pleistocene tusks (−0.064‰/degree) is similar to the modern meteoric water gradient (−0.064 to −0.048‰/degree). The temporal gradient in mean tusk $\delta^{18}O$ in Taimyr from an interstadial during MIS 3 to a stadial during MIS 2 (4.0‰) is similar to the gradient in easternmost Siberia from an interstadial during MIS 3 to the middle Holocene (4.8‰). Seasonality in Chukotka during the late Pleistocene does not appear to be different from that on Wrangel Island during the Holocene. Our results suggest that climate change as recorded by $\delta^{18}O$ values of mammoth tusks may not have been the direct cause of the extinction of Eurasian mammoths.

1. Introduction

The causes of the late Pleistocene extinction of diverse large-bodied mammals, including several species of proboscideans, on the northern continents remain a topic of debate (Martin and Klein, 1984; MacPhee, 1999; Barnosky et al., 2005). For many years, the primary end-member hypotheses explaining late Pleistocene extinctions, originally but no longer exclusively based on the North American record, have focused on either climatic and environmental changes associated with the last glacial–interglacial transition (e.g., Graham and Lundelius, 1984; Guthrie, 1984; Haynes, 1991; Lister and Sher, 1995) or overhunting by humans (e.g., Martin, 1967; Whittington and Dyke, 1984; Alroy, 2001; Fisher, 2001a). More recently, hyperdisease has been suggested as a cause (MacPhee and Marx, 1997), and a variety of mixed models combine elements of both climatic/environmental and overkill models (Owen-Smith, 1987; Haynes, 1991).

In the case of *Mammuthus primigenius* in Eurasia, Stuart (1991, 1999, 2005) has suggested a mixed model in which cooler conditions during the Allerød phase of the Late Glacial Interstadial (ca. 11.8–10.7 ka, all dates in radiocarbon years before present unless otherwise indicated) and

*Corresponding author. Tel.: +1 612 624 6361; fax: +1 612 625 3819.
E-mail addresses: dlfox@umn.edu (D.L. Fox), dcfisher@umich.edu (D.C. Fisher), sv@SV1226.spb.edu (S. Vartanyan), atikh@mail.ru (A.N. Tikhonov), dickmol@tiscali.nl (D. Mol), b.buigues@polarcircle.com (B. Buigues).

1040-6182/$ - see front matter © 2006 Elsevier Ltd and INQUA. All rights reserved.
doi:10.1016/j.quaint.2006.09.001

the expansion of boreal woodlands led to the restriction of *M. primigenius* to refugia in northern Eurasia (Taimyr and Gydan Peninsulas, the Severnaya Zemlya Archipelago, and Wrangel Island). Following a brief range expansion into northeastern Europe during the cold Younger Dryas (ca. 10.7–10.0 ka), radiocarbon dates suggest that the final extinction of mainland populations in Taimyr happened during the earliest Holocene and that of the remnant population on Wrangel Island not until the late Holocene (ca. 3.7 ka; Vartanyan et al., 1993, 1995; Long et al., 1994). In this model, the final extinctions were potentially caused by predation by technologically sophisticated modern human hunters that prevented migrations by stressed and reduced populations to physiologically and ecologically suitable refugia from latest Pleistocene and Holocene environmental changes.

In this paper, we use combined growth increment profiles and the stable oxygen isotope composition ($\delta^{18}O$) of serial samples of *M. primigenius* tusks from the Taimyr Peninsula, Chukotka (easternmost Siberia), and Wrangel Island, in conjunction with previously published isotopic results for mammoths from European Russia and central Siberia (Genoni et al., 1998), to explore aspects of climate change in northern and eastern Eurasia from the MIS 3 (Middle Weichselian) to the Middle Holocene (6.6–4.2 ka). Our approach allows us to examine temporal and spatial changes in both mean annual conditions and seasonal variation. This work is part of a larger project using growth increment and stable isotope profiles to understand both the paleobiology and the extinction of mammoths in Eurasia. Although the set of dated and analyzed tusks is relatively small at present ($n = 11$), the results suggest several climatic patterns that bear on the role of climate in the extinction of mammoths in northern Siberia. As the number of tusks analyzed increases, we will be able to test the climatic interpretations presented here with additional oxygen isotope data from both lattice-bound carbonate and phosphate in tusk apatite and complement the growth increment and oxygen isotope results with carbon isotope compositions from apatite carbonate and collagen, nitrogen isotope compositions of collagen, and strontium isotope compositions of apatite that will provide detailed paleobiological information. An expanded data set will also facilitate comparisons with other paleoclimatic and paleoenvironmental data from the region, such as the $\delta^{18}O$ value of permafrost and pollen records.

2. Mammoth tusks and tusk growth

Tusks are highly modified incisor teeth that form through a life-long history of growth, in response to complex interactions involving climate, food resources, behavior, and reproductive history (Fisher, 2001a; see also Rountrey et al., this volume). They are composed principally of dentin and cementum. Cementum is initially present over most of the tusk, but only as a thin, outer zone which is later reduced or removed by abrasion. The main tusk tissue is dentin, which is a composite material composed of hydroxyapatite, collagen, small proportions of other proteins, and water. Geometrically, tusks are stacks of cone-shaped layers added sequentially from tip to base. Tusk dentin is composed of a hierarchy of structural increments that parallel the conical pulp cavity and form on annual (first-order), weekly (second-order), and daily (third-order) timescales (Fisher, 2001a). The annual nature of first-order increments has been corroborated by $\delta^{18}O$ profiles in previous studies of serial samples of tusk dentin (Koch et al., 1998; Fisher et al., 2003; Fisher and Fox, 2003). First-order increments are reproducible within and between individuals and are identifiable by a variety criteria in addition to $\delta^{18}O$ profiles in individuals from highly seasonal climates: dentin color, topography of the dentin-cementum junction, and frequently the pattern of second-order thickness profiles, which can reflect seasonal variation in tusk growth rate. In high-latitude mammoths, the number of second-order increments per year varies from the typical temperate-latitude frequency of 52 per year to lower numbers that vary inversely with latitude. The explanation for this pattern is beyond the scope of this paper but probably relates to the interaction of different physiological rhythms associated with tusk growth and mineralization.

Increases in second-order increment thickness have been related to the nutritional and health status of the individual, and profiles of second-order increment thickness, in conjunction with criteria for recognizing first-order increments, can be used to identify winter–spring boundaries. We use the pattern of second-order increment thickness profiles from each tusk analyzed to identify the winter–spring boundary as the end of the thinnest second-order increment in a series of thin increments associated with a first-order increment boundary. Second-order increments provide a well constrained temporal framework for serial sampling of tusks for oxygen isotope composition of tusk apatite; the second-order thickness profiles and the winter–spring boundaries identified from them allow us to interpret subannual variations in the $\delta^{18}O$ profiles.

3. Oxygen isotope composition of Siberian mammoth tusk dentin

Both the lattice-bound or structural carbonate and the phosphate in mammalian tooth apatite form in oxygen isotope equilibrium with body water (Bryant et al., 1996; Iacumin et al., 1996). For this paper, we analyzed the oxygen isotope composition of structural carbonate in tusk dentin. The oxygen isotope composition of body water ($\delta^{18}O_{bw}$) in terrestrial mammals is controlled by the magnitude and composition of oxygen fluxes to and from body water (Luz et al., 1984; Bryant and Froelich, 1995; Kohn, 1996). Because the mineralized tissues in large mammals form at a constant body temperature (Cossins and Bowler, 1987), the only source of variation in the oxygen isotope composition of mammalian apatite

($\delta^{18}O_{ap}$) is the composition of body water ($\delta^{18}O_{bw}$). In mammals that ingest large volumes of water as drinking water or liquid water in plant stems, $\delta^{18}O_{bw}$ is sensitive to the oxygen isotope composition of meteoric water ($\delta^{18}O_{mw}$; Ayliffe et al., 1992; Kohn, 1996). Drinking water is derived from surface water reservoirs, and its $\delta^{18}O$ is largely controlled by $\delta^{18}O_{mw}$, with modification through evaporative enrichment in ^{18}O and local hydrologic processes. Liquid water in the stems of food plants is not fractionated relative to ground water and also reflects $\delta^{18}O_{mw}$ (Yakir, 1992), but leaf water in arid environments can be evaporatively enriched in ^{18}O relative to local meteoric water and the degree of enrichment increases with aridity (Sternberg et al., 1989). The effect of enriched leaf water on mammoth $\delta^{18}O_{ap}$ values is difficult to evaluate, but $\delta^{18}O_{ap}$ values of extant elephants *Loxodonta africana* and *Elephas maximus* have a strong, positive correlation with local $\delta^{18}O_{mw}$, and a least squares regression with local $\delta^{18}O_{mw}$ as the independent variable and elephant $\delta^{18}O_{ap}$ values as the dependent variable has a slope of 0.94 (Ayliffe et al., 1992). Additionally, a previous study of phosphate oxygen isotope variation in bulk samples of late Pleistocene Eurasian mammoth tusks, teeth, and bones suggests that mammoth $\delta^{18}O_{ap}$ values are a reasonable proxy for ancient $\delta^{18}O_{mw}$ values based on comparisons with $\delta^{18}O$ values of ice wedges and ground ice (Genoni et al., 1998).

Using $\delta^{18}O_{ap}$ values of serial samples of mammoth tusks as proxies for $\delta^{18}O_{mw}$ we can explore both temporal and spatial variation in $\delta^{18}O_{mw}$ during the late Pleistocene across Siberia and temporal variation from the late Pleistocene to the middle Holocene in easternmost Siberia (Chukotka and Wrangel Island). A recent study of the isotopic composition of meteoric water in Siberia (Siberia Network for Isotopes in Precipitation or SNIP; Kurita et al., 2004) includes sampling stations to the west and east of the Taimyr Peninsula (Salekhard and Olenek, respectively) and a coastal station in Chukotka (Ayon), thus providing modern precipitation data to assist our interpretations of mammoth data from central (Taimyr Peninsula) and eastern (Chukotka, Wrangel Island) Siberia. SNIP also includes stations in European Russia, which is one of the regions for which mammoth $\delta^{18}O$ values have been published (Genoni et al., 1998).

The three primary controls on the isotopic composition of meteoric water across Siberia today are precipitation history of air masses as they move across northern Eurasia from west to east, water vapor source, and temperature. We can use $\delta^{18}O_{ap}$ variations in our sample of mammoths to examine temporal and spatial variations in these factors in Siberia during the late Pleistocene and Holocene. At the continental scale, the primary circulation pattern is west to east transport of vapor across northern Eurasia from vapor sources in the Atlantic Ocean and the Norwegian and Baltic Seas (Kållberg et al., 2005). As an individual air mass moves across Eurasia, loss of moisture through continuous or sequential precipitation events leaves the remaining vapor progressively more depleted in the heavy isotopes of oxygen (and hydrogen) so that later precipitation events have systematically lower $\delta^{18}O$ values than earlier precipitation events (this is known as the continental effect; Rozanski et al., 1993). As a result of the continental effect, the primary spatial pattern of variation in modern $\delta^{18}O_{mw}$ values is a decrease in mean annual and mean winter $\delta^{18}O_{mw}$ values from west to east across Siberia (Kurita et al., 2004). For interior SNIP stations, the spatial pattern of mean annual and mean winter $\delta^{18}O_{mw}$ values can be accurately predicted by a Rayleigh distillation model in which $\delta^{18}O_{mw}$ at a given point along the trajectory of an air mass is a function of the $\delta^{18}O$ of the initial vapor, the fraction of initial vapor remaining, and the fractionation between vapor and liquid (Kurita et al., 2004).

In easternmost Siberia (Chukotka and Kamchatka), mean annual and mean winter $\delta^{18}O_{mw}$ do not correspond to the predictions of the Rayleigh model and have less negative $\delta^{18}O$ values than expected due to contributions of moisture from sources other than the Atlantic Ocean and the Norwegian and Baltic Seas. In easternmost Siberia, seasonal maps of wind vectors and moisture flux indicate that winter moisture is not derived from western sources but instead is derived from the North Pacific, with minor contributions from the nearby Arctic Ocean (Kållberg et al., 2005). These air masses have different initial vapor $\delta^{18}O$ values than western sources and experience little rainout before delivering moisture to Chukotka, and as a result have higher $\delta^{18}O$ values than predicted from the Rayleigh model assuming only eastward transport of moisture. We will use both our mammoth $\delta^{18}O_{ap}$ values reported here and values from the literature for localities across Russia and Siberia to examine whether patterns that characterized the late Pleistocene, particularly the Middle Weichselian interstadial (Sher et al., 2005), are consistent with this modern continental effect on meteoric water.

For non-coastal stations, mean annual hydrogen isotope composition of meteoric water (δD_{mw}), which has a strong, positive correlation with $\delta^{18}O_{mw}$ values for the same samples ($r = 0.99$), has a strong, positive correlation with mean annual temperature ($r = 0.94$; Kurita et al., 2004) that is similar to the pattern observed globally at mid- to high-latitude sites (Rozanski et al., 1993). On a seasonal basis, δD_{mw} (hence $\delta^{18}O_{mw}$) for winter precipitation also has a strong, positive correlation with temperature at interior stations in Siberia ($r = 0.93$; Kurita et al., 2004), but this relationship is much weaker during summer ($r = 0.55$) because of a low longitudinal gradient in summer temperatures across Siberia and the contribution of moisture from the landscape to air masses (see below). Given that analysis of second-order growth increments allows us to identify both annual increments of tusk growth and the included winter growth portions of each year, changes in mean tusk $\delta^{18}O$ values in a given region through time provide a proxy for changes in mean annual temperature, assuming that regional atmospheric circulation patterns were basically the same in the past as today.

Similarly, winter growth $\delta^{18}O_{ap}$ values provide a proxy for winter minimum temperature in a given region.

Although the isotopic composition of summer precipitation in Siberia does not correlate as strongly with temperature as does that of winter precipitation, all stations do exhibit seasonal variation in isotopic composition in which winter precipitation is depleted in the heavy isotope of H or O (hence has lower δ values) relative to summer precipitation. Seasonality in the isotopic composition of meteoric water increases from west to east as far as Yakutsk (Kurita et al., 2004) but is lower further east, presumably due to the interaction between seasonal variations in temperature and moisture sources. However, across more or less all of Siberia, summer precipitation has lower $\delta^{18}O$ values than predicted by the Rayleigh distillation model (Kurita et al., 2004). During warm summer months, evaporation from soils and evapotranspiration from plants contributes vapor from prior precipitation to air masses as they move from west to east across Siberia. The proportion of recycled moisture during summer is generally greater than 40% and can be greater than 80% in eastern Siberia (Kurita et al., 2004). Early in summer, both surface water reservoirs and soil water include relatively more water derived from melt of snow from the prior winter, which would be isotopically light. Recycling of this water into summer air masses today contributes to low summer $\delta^{18}O$ values in meteoric water in eastern Siberia, and the effect is enhanced because evaporation enriches the vapor in ^{16}O. We will use the seasonal pattern of $\delta^{18}O_{ap}$ in tusks to examine changes in the magnitude and pattern of seasonal variation in $\delta^{18}O_{mw}$ in the late Pleistocene of the Taimyr Peninsula and Chukotka and the middle Holocene of Wrangel Island. Previous studies of $\delta^{18}O_{ap}$ profiles in serial samples of North American mammoths have demonstrated seasonal variations up to almost 5‰ that correlate with patterns of seasonal growth in associated growth increment profiles (Koch et al., 1998; Fisher et al., 2003). To interpret the Siberian profiles, we will have to consider both regional variation in seasonal moisture sources and the possible role of long-term changes in the amount of recycled moisture during the summer, including the proportion of moisture derived from snow melt.

4. Materials and methods

4.1. Tusks

We have dated and analyzed the isotopic composition of serial samples of three tusks from the Taimyr Peninsula, two tusks from Chukotka and five tusks from Wrangel Island; we also include a single value for an additional dated tusk from the Taimyr Peninsula. We have samples of additional dated tusks from Taimyr and Chukotka that have not been analyzed for isotopic composition yet. The Jarkov mammoth from the Taimyr Peninsula was previously dated by accelerator mass spectrometry (AMS) at the R.J. van de Graaff Laboratory at Utrecht University, The Netherlands (Mol et al., 2001). The other tusks from Taimyr and those from Chukotka were dated by AMS at the Center for Accelerator Mass Spectrometry at Lawrence Livermore National Laboratory. The Wrangel Island tusks were dated conventionally at St. Petersburg State University, Russia (Vartanyan et al., 1995). Radiocarbon dates for the tusks are reported in Table 1 along with summaries of the $\delta^{18}O$ profiles from each tusk.

4.2. Tusk sampling

Tusk analyses reported here derive from well preserved specimens recovered from permafrost. In some cases the cementum layer on the outside of a tusk shows evidence of slight weathering (fine, longitudinal fracturing and lightening of surface coloration) associated with recent exhumation and/or transient exposure at some time in the past, but in all cases the dentin is solid, dense, cream-colored, and pristine in condition. Specimens from the Taimyr were collected by CERPOLEX/*Mammuthus* expeditions and were returned to a base of operations in the city of Khatanga, northern Taimyr, where they are stored

Table 1
Radiocarbon ages and summaries of serial samples from each tusk

Specimen	Location	Age (ka)	Lab no.	*n*	$\delta^{18}O_{ap}$ VSMOW		
					mean ± 1 s.d.	Max	Min
Jarkov	Taimyr	20.3 ± 0.15	UtC 8137-39	22	15.3 ± 1.29	17.4	12.6
2000/210	Taimyr	33.5 ± 0.4	CAMS 105532	27	19.3 ± 0.74	20.9	18.1
2000/271	Taimyr	42.9 ± 1.4	CAMS 105537	1	17.6		
2000/288	Taimyr	42.9 ± 1.4	CAMS 105539	25	18.4 ± 0.74	20.9	16.0
ZCHM-16	Chukotka	44.6 ± 1.6	CAMS 110335	39	19.1 ± 0.91	21.1	17.7
ZCHM-18	Chukotka	49.0 ± 2.0	CAMS 110327	43	17.6 ± 1.35	22.6	14.8
32M	Wrangel I.	4.12 ± 110	LU-4448	20	21.2 ± 1.04	23.3	19.4
9M	Wrangel I.	4.40 ± 40	LU-2756	20	21.1 ± 0.92	22.6	19.5
33M	Wrangel I.	6.19 ± 70	LU-4468	3	20.4 ± 0.29	20.7	20.2
34M	Wrangel I.	6.22 ± 50	LU-4471	15	21.4 ± 0.51	22.5	20.9
29M	Wrangel I.	6.56 ± 60	LU-4449	26	19.4 ± 0.88	21.7	18.2

at ca. −11 °C in an "ice cave" dug into the permafrost. Specimens from Chukotka and Wrangel Island were mostly not collected in their entirety, because of logistic restrictions, but samples were cut from the proximal ends of tusks and returned to a laboratory setting.

Sampling of the Taimyr tusks was conducted in Khatanga using a heavy-duty drill and specially designed coring bits to cut 2-cm diameter cores, perpendicular to the long axis of each tusk, at a series of positions along the length of the tusk. Spacing of cores was designed to sample the entire tusk, providing a comprehensive record of life history, but at this time, we are reporting data for only a single core per specimen. An entire core, passing through the center of a tusk and out the other side, contains a duplicate record (outer surface to central axis, in each direction) of ca. 6–10 years of an animal's life. Finished cores were enclosed in plastic bags to retard moisture loss but were allowed to dry slowly over the course of about one year. A narrow facet was then polished along a medial or lateral flank of the core to display the orientation of incremental features. Dentin laminae conform to former positions of the conical pulp cavity of the tusk and are organized as a series of nested cones along the tusk's structural axis. The apical angle of these cones varies during the life of the animal and tends to differ between males and females (larger in females). On the polished facet a cutting plane is marked to be perpendicular to most, if not all, laminae in the half of the core from the outer curve of the tusk. This cutting plane, transverse in anatomical orientation, is typically at an angle of 7–15° from the long axis of the core. The core is then sliced (with an Isomet low-speed, diamond wafering saw) to remove two slabs, each 5 mm thick, from the center of the cylindrical core, leaving two wedge-shaped "heels", or remainders, on either side. The heels are used to produce thin sections to document dentin increments, and the slabs are polished on both sides before they have any opportunity to deform because of humidity changes. Polishing proceeds through a series of carbide-grit, adhesive-backed papers, ending with a slurry of 5-μm laevigated alumina in kerosene. No water is used during cutting or polishing, as exposure of dry dentin to water induces significant volume change, distortion, and sometimes fracturing.

Samples from Chukotka and Wrangel Island were either round segments or wedge-shaped sectors cut from the proximal end of tusks. These were also oriented and sliced with the Isomet into 5-mm thick slabs perpendicular to dentin laminae. These again were polished on both sides, while additional samples were trimmed for thin section production. In the case of cores and these more irregularly shaped samples, slabs were doubly polished because we are looking for the best display of fine, second-order (weekly) increments to guide the milling of serial isotope samples. The ease with which incremental features can be traced can vary unpredictably from one surface to another, so it is useful to be prepared to sample from either side of the polished slabs.

4.3. Growth increment analysis

Thin sections made from the "heels" remaining after slicing tusk cores for production of 5-mm slabs are given a final high-speed polish with 5-μm laevigated alumina in kerosene (Fisher, 2001a) and stored in plastic bags in an air-conditioned environment to minimize moisture uptake. Prior to microscopic analysis, thin sections are inspected and boundaries of first-order (annual) features are marked, based on discontinuities in dentin color, translucency, and locations of prominent (high-contrast) second-order features. Analysis of dentin increments is performed on a petrographic microscope, using Optimas 5.2 image analysis software. A transect overlay is constructed perpendicular to incremental features, and the dark portion of each second-order couplet is marked onscreen. Numbers and positions of second-order increments are exported to a spreadsheet, compiled (from the multiple transects required to analyze a given sequence), and graphed to yield profiles of second-order increment thickness.

Some years from these tusks resemble patterns observed in temperate-latitude mammoths, with 52 ± 3 second-order increments per first-order increment and 7 ± 1 third-order increments per second-order increment, where third-order increments can be adequately discerned. In these cases, we can interpret second-order features as periodic, and their thickness as a direct measure of short-term rate of dentin apposition. However, as discussed in Fisher and Fox (2003), other years in high-latitude mammoths, including especially the last years of life, often show fewer than 52 increments and, at least locally within the year, 11 ± 1 third-order increments per second-order increment. In these cases, we suspect second-order increments do not represent a single period of formation, and to interpret their thicknesses as a direct measure of tusk growth rate, we would have to distinguish carefully parts of the year characterized by different periodicities and impose an appropriate transformation on measured increment thicknessses. We are currently developing improved means of visualizing third-order increments to support such analyses, but for now, we must work simply with "raw" second-order increment data. This complex system has been provisionally interpreted as reflecting interaction between mammoths' circadian rhythms, responsible ultimately for third-order increments, and other periodicities associated with dentin mineralization (Fisher, 2001b). The different modes of organization observed (i.e., ca. 52/yr vs. <52/yr) may in turn represent times when mammoths were living below, and north of, the Arctic Circle, where certain times of the year may be characterized by circadian rhythms that become free-running, rather than entrained to 24-h light–dark cues (Fisher, 2001b).

The complication introduced by tracing profiles of increment thickness when the increments do not reflect a single periodicity compromises our ability to interpret increment profiles in terms of tusk growth rate, especially since we provisionally identify winter as a time when the

increment period may have been longer, making the apparent growth rate (i.e., without accounting for the change in period) greater than it actually was. "Spring," on the other hand, would have featured the return of 24-h light–dark cues, entrained circadian rhythms, shorter (weekly) second-order periodicity, and thus thinner second-order increments. In terms of growth conditions, this might still effectively represent "late winter." At high latitudes, where the start of the short growing season would be delayed relative to this transition, we may thus expect a functional "winter–spring" boundary to be associated with a transition from thin to thicker second-order increments. For now, we follow this convention.

4.4. Serial sampling for stable isotope analysis

Temporally discrete samples were extracted in series from each polished 5 mm thick sample slab under microscopic observation by following incremental features with a carbide steel dental bit with a cutting head that is 0.6 mm in diameter and 3.0 mm long mounted in a fixed dental drill. Milling of sample series began either at the pulp cavity surface and progressed outward toward the dentin-cementum junction or (for more distal slabs that did not have a pulp cavity surface) at a prominent growth line or set of lines between the axial trace and the dentin-cementum junction and then in both adaxial and abaxial directions. For individual samples, the stage was raised to plunge the bit shallowly into the transverse face of the slab at one end of the sample path, and the slab was then translated horizontally on the microscope stage to begin milling the sample using second order growth increments as guides to minimize temporal mixing between successive samples. Raising the stage for successive passes along the initial shallow sample path increased the depth of the groove until 40–60 mg of dentin powder had been collected. Successive samples were begun on opposite edges of the slab and each sample extended only slightly more than half way across the slab circumferentially to overlap with the end of the previous sample along the radial midline of the slab. With this sampling scheme, each sample position included both a powder sample from the milled groove and a block sample from the wall left between successive samples on either side of the sample block. One aliquot of each powder sample was processed for the oxygen isotope analyses of structural carbonate presented here; the remainder of each powder sample was retained for future analysis of phosphate oxygen and possibly other analyses (e.g., strontium isotopic and/or elemental composition). The block samples were processed for carbon and nitrogen isotope analyses of purified collagen; these results will be presented in a separate paper that includes the carbon isotope data from structural carbonate.

The radial thickness of individual samples was measured on high magnification ($>40\times$) digital photographs using NIH Image image analysis software. As samples follow incremental lines and the tusks are not perfectly circular, the thickness of each sample varies slightly along the sample path. Sample thicknesses were measured in a radial transect along the overlap zone for successive samples in the middle of each sample block where the adaxial margin of one sample forms the abaxial margin of the next sample farther from the dentin-cementum junction. The thicknesses of successive samples were added to obtain cumulative distances from the pulp cavity (expressed in negative units); isotope results from each sample are plotted at the middle of its measured thickness. When plotted in the spatial domain against cumulative distance from the pulp cavity, the oxygen isotope profile from a sample slab can be directly compared to the growth increment thickness profile derived from the thin section of the same block.

4.5. Stable oxygen isotope analyses

Given the pristine preservation of the dentin in all of these tusks, we followed the basic protocol of Stephan (2000) to purify powder samples of collagen-rich apatite for stable isotope analysis of the structural carbonate. A 25 mg aliquot of each powder sample was soaked in 2 ml of 2–3% NaOCl for 24 h to dissolve collagen and any sedimentary organic matter, then rinsed five times in an excess of distilled water. The samples were then soaked for 24 h in 2 ml of 0.125 N NaOH to dissolve any humic or fulvic acids, rinsed an additional five times in an excess of distilled water, and then freeze-dried for at least 12 h. Samples were not treated with acetic acid as in the protocol of Koch et al. (1997) because the tusks are geologically young and are so well-preserved as to be fresh ivory; thus we are not concerned with contamination by sedimentary carbonate. Futhermore, results presented here suggest that contamination with sedimentary carbonate has not occurred. The carbon and oxygen isotope compositions of the purified carbonate samples were measured using a Finnigan "Kiel" automatic extraction line coupled to the ion source of a Finnigan MAT 252 isotope ratio mass spectrometer in the Stable Isotope Laboratory in the Department of Geology and Geophysics at the University of Minnesota. Sample values are normalized to the compositions of National Bureau of Standards carbonate standards NBS-18 and NBS-19 and two laboratory standards, and analytical precision is better than 0.1‰.

5. Results

Mean, standard deviation, maximum, and minimum $\delta^{18}O_{ap}$ values for the sample series from each tusk are presented in Table 1 and second-order increment and $\delta^{18}O_{ap}$ profiles are presented in Figs. 1–3 for representative results from the Taimyr Peninsula and Wrangel Island and for both tusks from Chukotka. We briefly summarize the results for each region below. The full data set is available from the corresponding author upon request.

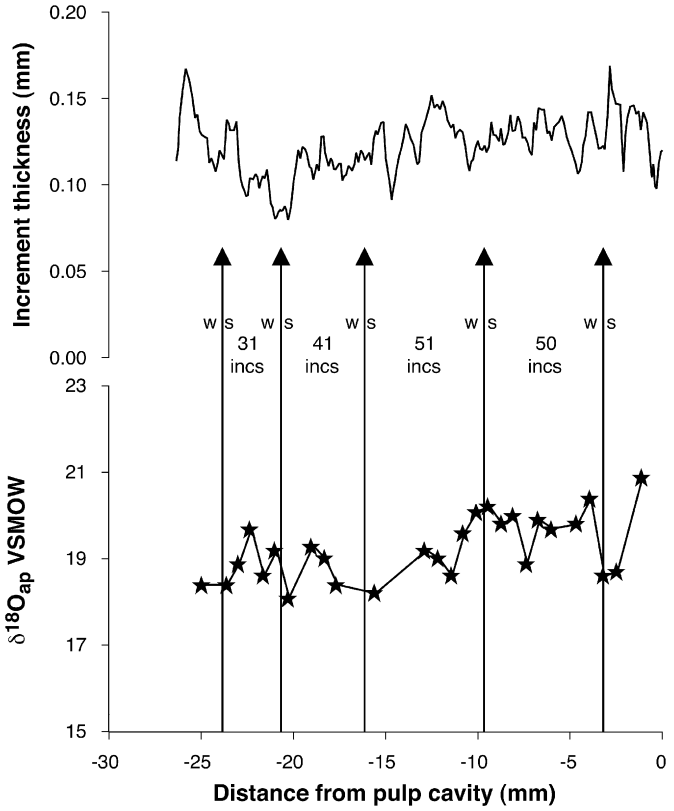

Fig. 1. Growth increment and $\delta^{18}O$ profiles for tusk 2000/210 from CERPOLEX/*Mammuthus* collections from the Taimyr peninsula (south of Cape Sablera, Lake Taimyr). Vertical lines with arrows indicate positions of winter–spring boundaries with the number of second-order increments indicated. In each plot, earlier portions of life are to the left (i.e., time runs from left to right).

5.1. Taimyr Peninsula

The Taimyr sample includes tusks from three climatically distinct intervals. Based on the calibration curve of Fairbanks et al. (2005), the two oldest tusks from the Taimyr Peninsula, 288 and 271 (for which we only have a single value currently), are from just after the peak of interstadial 13 during MIS 3 in the Greenland ice cores, but before the peak of stadial 13 and Heinrich event 5 in the North Atlantic (Bond et al., 1993; Dansgaard et al., 1993). Thus, these tusks correspond to a moderate global climate state. During this interval, northern Siberia to the east of the Taimyr Peninsula was characterized by warm steppe-tundra floras, summers that were dry and warmer than present, and winters that were colder than present (Middle Weichselian I; Sher et al., 2005). The single value for 271 (17.6‰) is lower than the mean for 288 (18.4 ± 0.74, 1 s.d.) but falls well within the range of the more complete series from 288 (20.9–16.0‰). The calibrated age for the next younger tusk, 210, corresponds to Greenland interstadial 8, just after Heinrich event 4 (Bond et al., 1993; Dansgaard et al., 1993). The Greenland ice records have higher $\delta^{18}O$ during this interval than that corresponding to the two older tusks from the Taimyr Peninsula (Dansgaard et al., 1993); thus 210 derives from a climate that was somewhat warmer globally. In north central Siberia, this interval (Middle Weichselian I; Sher et al., 2005) was also characterized by warm steppe-tundra and summers that were cooler than during the Middle Weichselian II interval but still warmer than present. Although the range for 210 (20.9–18.1‰) completely overlaps with that from the older 288, the mean value for 210 (19.3 ± 0.74) is about 1‰ higher than that for 288, which is consistent with the higher $\delta^{18}O$ values in the Greenland ice cores during interstadial 8. Jarkov is the youngest tusk from the Taimyr Peninsula and dates to before the last glacial maximum during MIS 2. The calibrated age of Jarkov corresponds to the lowest $\delta^{18}O$ values of stadial 3 in the Greenland ice sheet (Dansgaard et al., 1993). This interval is the Sartanian stadial (Late Weichselian) in north-central Siberia, which is characterized by cold tundra-steppe and cold, dry summers (Sher et al., 2005). Mean $\delta^{18}O$ for Jarkov (15.3 ± 1.29‰) is 3–4‰ lower than the values for the other tusks from the Taimyr Peninsula, which is consistent with colder conditions globally recorded in the Greenland ice sheet. The $\delta^{18}O$ profile for Jarkov is also more variable than the other tusks.

None of these tusks exhibit coherent patterns of seasonal variation in either second-order increment or $\delta^{18}O$ profiles such as have been seen in *Mammuthus* from mid-continental North America (Koch et al., 1998; Fisher et al., 2003). It is beyond the scope of this paper to address evidence and arguments for multiannual migrations by Siberian mammoths (Fisher and Beld, 2002), but such behavior could be a confounding factor for both growth increment and $\delta^{18}O$ profiles from the Taimyr tusks. However, growth increments clearly indicate that the last two years of life in 288 (Fig. 1) do not exhibit strong seasonality in either tusk growth or $\delta^{18}O$ values. The results from the three Taimyr series are climatically coherent: the highest $\delta^{18}O$ values are for a tusk from an interstadial during MIS 3, the intermediate values are for a tusk from a stadial during MIS 3, and the lowest values are for a tusk from MIS 2 just before the Last Glacial Maximum. Warmer intervals thus appear to have been characterized by higher $\delta^{18}O_{mw}$ as expected, which led to higher mammoth $\delta^{18}O_{ap}$.

5.2. Chukotka

Results for the two tusks from Chukotka (ZCHM-18 and -16; Fig. 2) have quite similar growth increment and $\delta^{18}O$ profiles. The radiocarbon age for the older of the two Chukotka tusks, ZCHM-18, is beyond the range of the calibration curve of Fairbanks et al. (2005). The younger tusk, ZCHM-16, has a calibrated age that falls between the peak of Greenland interstadial 14 and stadial 14. ZCHM-16 has higher mean $\delta^{18}O_{ap}$ (19.1 ± 0.74‰) and a lower range (3.4‰) than the older ZCHM-18 (17.6 ± 1.35 and 7.8‰, respectively). Both tusks correspond to the early part of the Middle Weichselian I phase of MIS 3 in north-central Siberia, characterized by warm steppe-tundra,

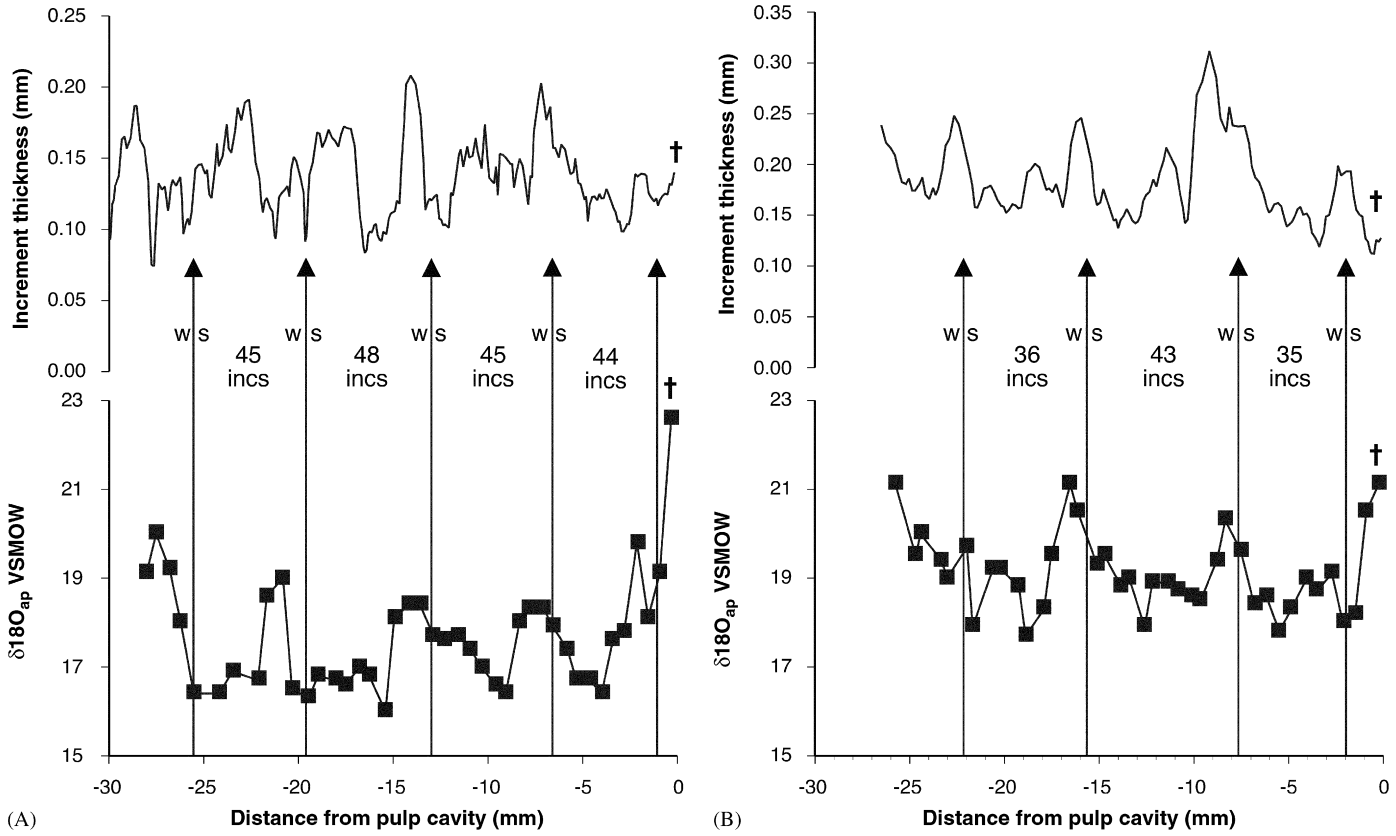

Fig. 2. Growth increment and $\delta^{18}O$ profiles for (A) ZCHM-18 and (B) ZCHM-16 from Chukotka. Vertical lines with arrows indicate positions of winter–spring boundaries with the number of second-order increments indicated. In each plot, earlier portions of life are to the left and time of death is marked by the dagger at the sample from the pulp cavity surface.

summers that were dry and warmer than today, and winters that were colder than today (Sher et al., 2005). Based on the correspondence between mean $\delta^{18}O$ values of the Taimyr Peninsula tusks and the conditions recorded by the Greenland ice sheet discussed above in Section 5.1, we suspect that ZCHM-18 derives from a cooler interval than ZCHM-16, but this is hard to assess given the old radiocarbon age of ZCHM-18. Additionally, we cannot determine whether the greater variability in ZCHM-18 is characteristic of a different climatic interval in easternmost Siberia or if it is only due to normal interannual variability. Unlike the Taimyr tusks, the growth increment and $\delta^{18}O$ profiles from both Chukotka tusks exhibit regular seasonal variations. Surprisingly, in most years in both tusks, the highest $\delta^{18}O$ values occur in late winter, just before the winter–spring boundary. In North American *Mammuthus* tusks with seasonal variations in $\delta^{18}O$, high values correspond to summer based on second-order growth increments (Koch et al., 1998; Fisher et al., 2003). We discuss possible explanations for the high winter $\delta^{18}O$ values in Section 6.

5.3. Wrangel Island

The five Wrangel Island tusks are all from the middle Holocene, with three of them clustered in age around 6.5 ka and two of them close to 4.3 ka (Table 1). Variation in mean $\delta^{18}O$ value among the five tusks does not appear to correlate with age as the highest mean ($21.4 \pm 0.51‰$) is for tusk 34M, dated to 6.2 ka, and the lowest mean ($19.4 \pm 0.88‰$) is for the oldest tusk we analyzed from Wrangel Island, 29M, which is dated to 6.6 ka. In general, mean $\delta^{18}O$ values among the Wrangel tusks are similar, and the ranges of values from all five tusks overlap. Growth increment profiles (Fig. 3) are generally seasonal in character with highest growth rates during summer, but a mid-year drop in growth rate appears to be common. Oxygen isotope profiles from Wrangel Island appear to fall into two modalities. Three of the tusks exhibit $\delta^{18}O$ profiles like that in 9M, which has a somewhat irregular pattern that might be like the typical North American pattern with high values during summer and early fall but occasional unusually low values that make a strictly seasonal pattern hard to discern. 29M exhibits a more regular seasonal $\delta^{18}O$ profile (with a superimposed trend toward higher values over the last couple years of life) but with the same inverse seasonal pattern of higher winter $\delta^{18}O$ values exhibited by the two tusks from Chukotka. The Holocene global hydrologic cycle was isotopically lighter than the late Pleistocene cycle due to the contribution of ^{16}O from melted ice sheets. To be comparable to the Pleistocene data, values for the Wrangel Island tusks should be

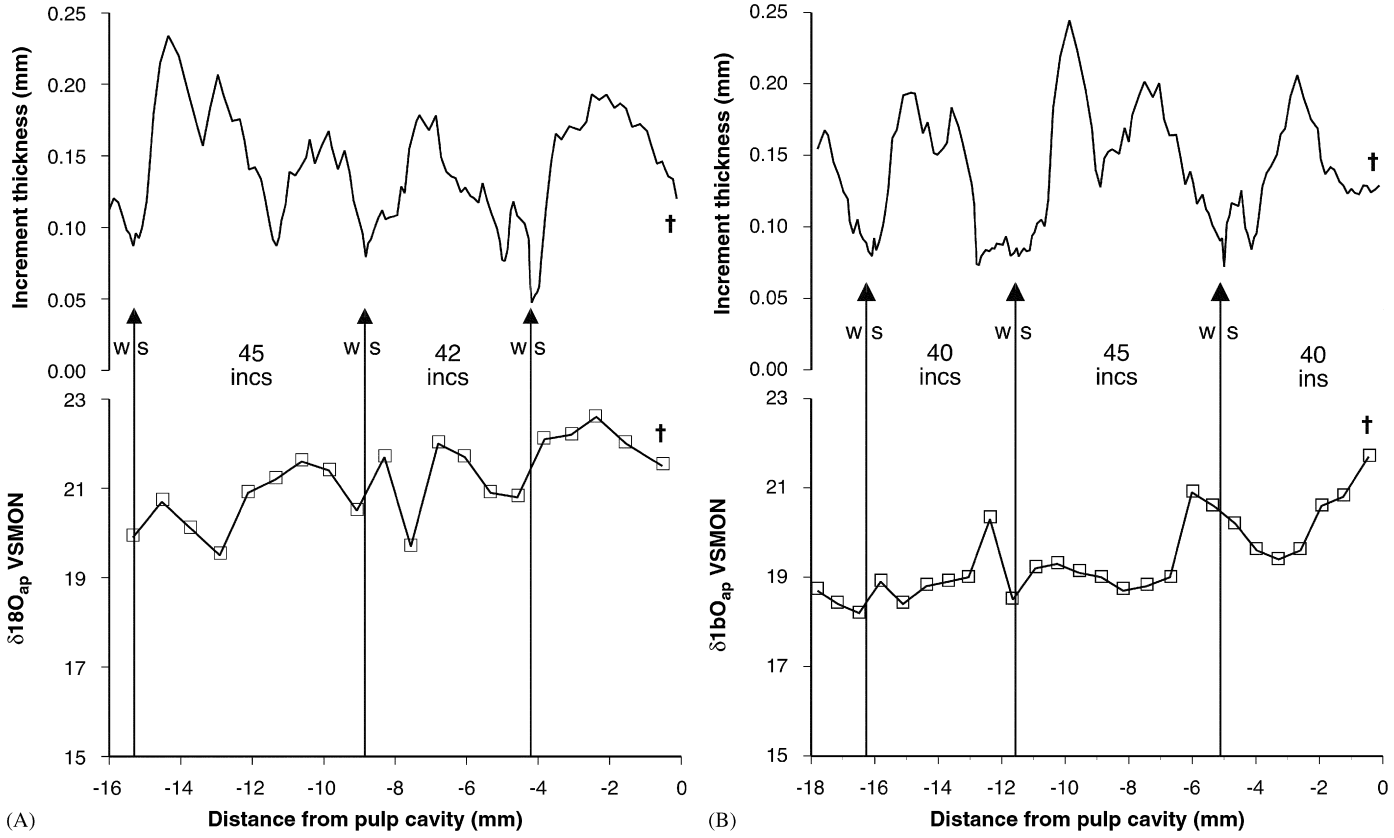

Fig. 3. Growth increment and $\delta^{18}O$ profiles for (A) 9M and (B) 29M from Wrangel Island. Vertical lines with arrows indicate positions of winter–spring boundaries with the number of second-order increments indicated. In each plot, earlier portions of life are to the left and time of death is marked by the dagger at the sample from the pulp cavity surface.

adjusted higher by about 1‰ to account for the difference in ice volume from the late Pleistocene to the Holocene.

6. Discussion and conclusions

Our results do not suggest that in years sampled any of the animals migrated long distances latitudinally. Given that all years sampled in these animals had fewer than 52 second-order increments, we suspect that all animals were resident at high latitude during these years and that latitudinal variation in the $\delta^{18}O$ of meteoric water is not a prominent factor in the data presented here. Full series of samples from entire life histories might reveal longer-term variations in isotopic composition that reflect patterns of interannual latitudinal migration.

Three aspects of our results are particularly striking and potentially bear on the role of climate change in the extinction of *M. primigenius* during the late Pleistocene on the mainland and the middle Holocene on Wrangel Island. First, the spatial gradient in late Pleistocene mammoth $\delta^{18}O$ values across Siberia is remarkably similar to the spatial gradient in $\delta^{18}O_{mw}$ values today (Fig. 4; Kurita et al., 2004). Considering only the higher latitude ($>60^\circ$ N) SNIP stations (which have lower $\delta^{18}O$ values than the lower latitude stations due to the latitudinal gradient in temperature), the longitudinal gradient in mean annual $\delta^{18}O_{mw}$ values is -0.064‰/degree of longitude and the decrease in $\delta^{18}O_{mw}$ from west (northern Ukraine/Russia) to east (northeastern Yakutia) is about 8‰. The regression of $\delta^{18}O_{mw}$ values as the dependent variable on longitude as the independent variable is statistically significant ($p = 0.03$) even though the number of stations (6) is small. If all stations, not only those at higher latitude, are included ($n = 13$), the regression is not significant ($p = 0.08$) and the gradient is slightly less ($-0.048/^\circ$ longitude). In either case, the decrease in $\delta^{18}O_{mw}$ with longitude is due primarily to the continental effect, as discussed in Section 3. Although the easternmost higher latitude SNIP station (Ayon) has the most negative $\delta^{18}O$ values, they are actually less negative than expected from the Rayleigh distillation model due to the influence of moisture derived from nearby marine sources (northern Pacific and Arctic Oceans; Kurita et al., 2004).

Without accounting for variations in age among the samples from each region, the longitudinal gradient in mammoth $\delta^{18}O$ values from sites in the Ukraine and European Russia to Yakutia is evident, as is the deviation to higher values of the two mammoths from Chukotka. Genoni et al. (1998) published $\delta^{18}O$ values of mammoth apatite phosphate, which is systematically lower than corresponding apatite carbonate values by about 8.7‰ (Bryant et al., 1996; Iacumin et al., 1996). We used least

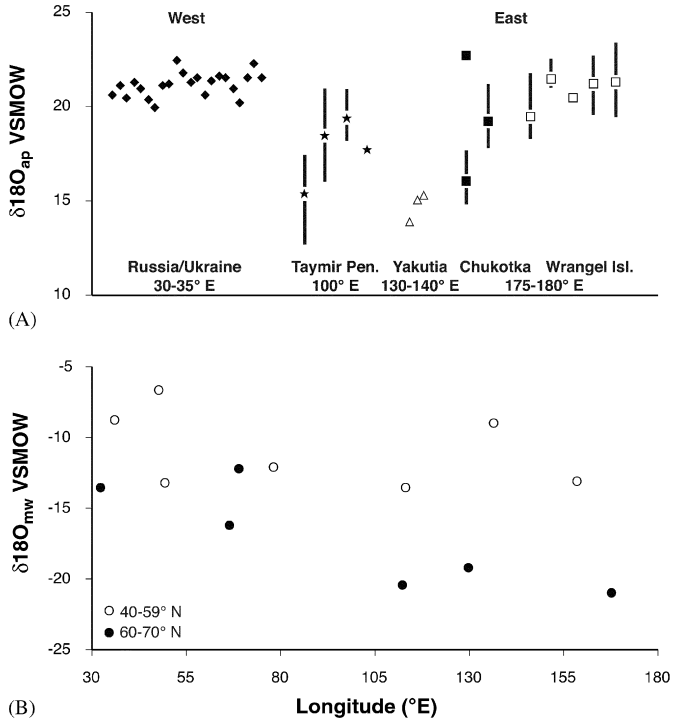

Fig. 4. Spatial variation in $\delta^{18}O$ values of (A) Siberian mammoths and (B) modern meteoric water in Siberia. Mammoth data from Ukraine/Russia and Yakutia from Genoni et al. (1998) are from PO_4 and converted to equivalent CO_3 values using data from Bryant et al. (1996) and Iacumin et al. (1996). Approximate longitude of samples from each region is indicated. Meteoric water data from Kurita et al. (2004).

squares linear regression of paired phosphate and carbonate $\delta^{18}O$ values of modern mammals in Bryant et al. (1996) and Iacumin et al. (1996) to transform the phosphate $\delta^{18}O$ data in Genoni et al. (1998) into the equivalent carbonate $\delta^{18}O$ values; the 95% confidence interval for the slope of the regression (± 0.03) is much smaller than the range of variation in the mammoth data discussed here. The mean value for the Ukraine/Russian data from Genoni et al. (1998) is 21.1 ± 0.63‰ and the range in the data (2.4‰), despite ages for sites that range from 24.3 to 14.3 ka, is comparable to the variation within each of our tusk series. The mean $\delta^{18}O$ for the four Taimyr tusks is 17.7‰. The mean $\delta^{18}O$ for the three Yakutian samples from Genoni et al. (1998) is 14.7‰, and, again despite the age range in the samples (10 to >40 ka), the range among the three values is less than in all of the individual tusk series. The samples from these three regions span approximately 100° of longitude, so the gradient across them is −0.064‰/degree, almost exactly the same as the gradient in modern $\delta^{18}O_{mw}$ values. This result suggests that the relationship between mammoth $\delta^{18}O_{ap}$ values and local meteoric water has a slope close to 1.0, as is the case for modern elephants (0.94; Ayliffe et al., 1992). The positive deviation of the mean values from Chukotka relative to the trend for the more westerly sites is also similar to the modern meteoric water pattern. Thus, our results suggest that at the continental scale, the pattern of moisture transport across Eurasia and the intensity of the continental effect on meteoric water isotopic composition during the late Pleistocene was probably similar to modern patterns. As our data set expands with analyses of additional dated tusks, we should be able to examine how the gradient varied through time with greater resolution.

Second, the pattern of seasonality of $\delta^{18}O$ values in Chukotka during MIS 3 was similar to the pattern on Wrangel Island during at least some parts of the middle Holocene. We attribute the unexpected pattern of higher $\delta^{18}O$ values during winter to two factors. Today, winter precipitation in easternmost Siberia includes a large component of moisture derived from the nearby northern Pacific and/or the Arctic Ocean that would not have become depleted in ^{18}O through rain-out and thus would have higher $\delta^{18}O$ values than expected based on air temperature and the Rayleigh distillation model for Atlantic-derived moisture. However, winter precipitation in Ayon in western Chukotka still has lower $\delta^{18}O$ values than summer precipitation. A second factor is the amount of recycled moisture included in summer precipitation, which has a negative correlation with $\delta^{18}O_{mw}$ of summer precipitation today (Kurita et al., 2004). A larger contribution of winter snow melt to the recycled water, as might be expected during MIS 3 and even episodically at times during the Holocene on Wrangel Island, and warmer, drier summers with enhanced surface evaporation (which would preferentially move ^{16}O into vapor) would both yield recycled moisture with a lower $\delta^{18}O$ value. Given that summer $\delta^{18}O_{mw}$ values would be low because of the continental effect anyway, it is possible that greater winter snow melt and increased surface evaporation could actually yield summer $\delta^{18}O_{mw}$ values that were lower than winter values (hence the seasonality patterns in ZCHM-18 and -16 and 29M) despite higher air temperatures than in winter. The similarity between the seasonality patterns for some of the tusks from easternmost Siberia also suggests some degree of climatic continuity in the region from the late Pleistocene to the middle Holocene.

Finally, the temporal gradients in mean $\delta^{18}O$ values in Taimyr and in easternmost Siberia, which should be a proxy for changes in mean annual temperature in each region, are similar over different climatic intervals. Considering only mean $\delta^{18}O_{ap}$ values, the temporal gradient in Taimyr from interstadial conditions during MIS 3 (210, 19.3‰) and conditions close to a stadial in MIS 2 prior to the glacial maximum (Jarkov, 15.3‰) is 4‰. Correcting for the ice volume effect on the Wrangel tusks, the temporal gradient in easternmost Siberia from the lowest mean $\delta^{18}O$ for MIS 3 (ZCHM-18, 17.6‰) to the highest value for Wrangel Island (34M, 21.4‰ measured, 22.4‰ adjusted) is 4.8‰. If we use the mean values for all of the individual samples from both Chukotka tusks (18.4‰) and all five Wrangel tusks (20.7‰), the difference is only 2.3‰. From these data, it appears that the degree of climate change recorded by tusks in easternmost Siberia from the

interstadial conditions of MIS 3/Middle Weichselian to the middle Holocene may have been about the same as the degree of climate change from MIS 3/Middle Weichselian to the last glacial maximum in the Taimyr Peninsula.

We propose that climate alone was not a driving factor behind the extinction of *M. primigenius* in Eurasia during either the late Pleistocene or the late Holocene. Our results obviously do not rule out floral changes in response to climate change as a cause, nor human hunting in combination with range and population size reductions. Of course, survival of *M. primigenius* on Wrangel Island across the glacial–interglacial transition at the end of the Pleistocene and into the middle Holocene by itself implies that climate change and absolutely warmer Holocene conditions in eastern Siberia were not sufficient to cause extinction of mammoths. We will need to test these patterns with more data from tusks from Siberia and augment our interpretations with additional paleobiological information from carbon and nitrogen isotope profiles from these and other tusks, but observations reported here already raise issues that must be addressed by climate-driven models of the extinction process.

References

Alroy, J., 2001. A multispecies overkill simulation of the end-Pleistocene megafaunal mass extinction. Science 292, 1893–1896.

Ayliffe, L.K., Lister, A.M., Chivas, A.R., 1992. The preservation of glacial–interglacial climatic signatures in the oxygen isotopes of elephant skeletal phosphate. Palaeogeography, Palaeoclimatology, Palaeoecology 99, 179–191.

Barnosky, A.D., Koch, P.L., Feranec, R.S., Wing, S.L., Shabel, A.B., 2005. Assessing the causes of Late Pleistocene extinctions on the continents. Science 306, 70–75.

Bond, G., Broecker, W., Johnsen, S., McManus, J., Labeyrie, L., Jouzel, J., Bonani, G., 1993. Correlations between climate records from North Atlantic sediments and Greenland ice. Nature 365, 143–147.

Bryant, J.D., Koch, P.L., Froelich, P.N., Showers, W.J., Genna, B.J., 1996. Oxygen isotope partitioning between phosphate and carbonate in mammalian apatite. Geochimica et Cosmochimica Acta 60, 5145–5148.

Dansgaard, W., Johnsen, S.J., Clausen, H.B., Dahl-Jensen, D., Gundestrup, N.S., Hammer, C.U., Hvidberg, C.S., Steffensen, J.P., Sveinbjörnsdottir, A.E., Jouzel, J., Bond, G., 1993. Evidence for general instability of past climate from a 250-kyr ice-core record. Nature 364, 218–220.

Fairbanks, R.G., Mortlock, R.A., Chiu, T., Cao, L., Kaplan, A., Guilderson, T.P., Fairbanks, T.W., Bloom, A.L., Grootes, P.M., Nadeau, M.J., 2005. Radiocarbon calibration curve spanning 0–50,000 years BP based on paired $^{230}Th/^{234}U/^{238}U$ and ^{14}C dates on pristine corals. Quaternary Science Reviews 24, 1781–1796.

Fisher, D.C., 2001a. Season of death, growth rates, and life history of North American mammoths. In: West, D. (Ed.), Proceedings of the International Conference on Mammoth Site Studies. Publications in Anthropology 22. University of Kansas, Lawrence, KS, pp. 121–135.

Fisher, D.C., 2001b. Entrained vs. free-running physiological rhythms and incremental features in the tusks of woolly mammoths. Journal of Vertebrate Paleontology 21 (Suppl. 3), 49A–50A [Abstract].

Fisher, D.C., Beld, S.G., 2002. Whole-tusk growth records of late Pleistocene woolly mammoth from the Taimir Peninsula, Siberia. Journal of Vertebrate Paleontology 22 (Suppl. 3), 53A [Abstract].

Fisher, D.C., Fox, D.L., 2003. Season of death and terminal growth histories of Hiscock mastodons. In: Laub, R.S., (Ed.), The Hiscock Site: Late Pleistocene and Holocene Paleoecology and Archaeology in Western New York State. Bulletin of the Buffalo Society of Natural Sciences 37, 83–100.

Fisher, D.C., Fox, D.L., Agenbroad, L.D., 2003. Tusk growth rate and season of death of *Mammuthus columbi* from Hot Springs, South Dakota, USA. Deinsea 9, 117–133.

Genoni, L., Iacumin, P., Nikolaev, V., Gribchenko, Y., Longinelli, A., 1998. Oxygen isotope measurements of mammoth and reindeer skeletal remains: an archive of Late Pleistocene environmental conditions in Eurasian arctic. Earth and Planetary Science Letters 160, 587–592.

Graham, R.W., Lundelius, E.L., 1984. Coevolutionary disequilibrium and Pleistocene extinctions. In: Martin, P.S., Klein, R.G. (Eds.), Quaternary Extinctions: A Prehistoric Revolution. University of Arizona Press, Tuscon, pp. 223–249.

Guthrie, R.D., 1984. Mosaics, allochemics, and nutrients: an ecological theory of late Pleistocene megafaunal extinctions. In: Martin, P.S., Klein, R.G. (Eds.), Quaternary Extinctions: A Prehistoric Revolution. University of Arizona Press, Tuscon, pp. 259–298.

Haynes, C.V., 1991. Geoarchaeological and paleohydrological evidence for a Clovis-age drought in North America and its bearing on extinction. Quaternary Research 35, 438–450.

Haynes, G., 1991. Mammoths, Mastodonts, and Elephants: Biology, Behavior, and the Fossil Record. Cambridge University Press, Cambridge, 413p.

Iacumin, P., Bocherens, H., Mariotti, A., Longinelli, A., 1996. Oxygen isotope analyses of co-existing carbonate and phosphate in biogenic apatite: a way to monitor diagenetic alteration of bone phosphate? Earth and Planetary Science Letters 142, 1–6.

Kållberg, P., Berrisford, P., Hoskins, B., Simmons, A., Uppala, S., Lamy-Thépaut, S, Hine, R., 2005. ERA-40 Atlas. ERA-40 Project Report Series No. 19. European Centre for Medium Range Weather Forecasts, Reading, England, 103pp.

Koch, P.L., Tuross, N., Fogel, M.L., 1997. The effects of sample treatment and diagenesis on the isotopic integrity of carbonate in biogenic hydroxylapatite. Journal of Archaeological Science 24, 417–429.

Koch, P.L., Hoppe, K.A., Webb, S.D., 1998. The isotopic ecology of late Pleistocene mammals in North America Part 1. Florida. Chemical Geology 152, 119–138.

Kohn, M., 1996. Predicting animal $\delta^{18}O$: accounting for diet and physiological adaptation. Geochimica et Cosmochimica Acta 60, 4811–4829.

Kurita, N., Yoshida, N., Inoue, G., Chayanova, E.A., 2004. Modern isotope climatology of Russia: a first assessment. Journal of Geophysical Research 109, D03102.

Lister, A.M., Sher, A.V., 1995. Ice cores and mammoth extinction. Nature 378, 23–24.

Long, A., Sher, A.V., Vartanyan, S.L., 1994. Holocene mammoth dates. Nature 369, 364.

MacPhee, R.D.E. (Ed.), 1999. Extinctions in Near Time: Causes, Contexts, and Consequences. Kluwer/Plenum, New York.

MacPhee, R.D.E., Marx, P.A., 1997. The 40,000-year plague: humans, hyperdisease and first-contact extinctions. In: Goodman, S., Patterson, D. (Eds.), Natural Change and Human Impact in Madagascar. Smithsonian Institution Press, Washington, DC, pp. 169–217.

Martin, P.S., 1967. Prehistoric overkill. In: Martin, P.S., Wright, H.E. (Eds.), Pleistocene Extinctions: The Search for a Cause. Yale University Press, New Haven, pp. 75–120.

Martin, P.S., Klein, R.G. (Eds.), 1984. Quaternary Extinctions: A Prehistoric Revolution. University of Arizona Press, Tucson.

Mol, D., Coppens, Y., Tikhonov, A., Agenbroad, L.D., MacPhee, R., Flemming, C., Buigues, B., de Marliave, C., van Geel, B., van Reenen, G., Pals, J.P., Fisher, D.C., Fox, D.L., 2001. The Jarkov Mammoth: 20,000-year-old carcass of a Siberian woolly mammoth *Mammuthus primigenius* (Blumenbach, 1799). In: Cavarretta, G., Giola, P., Mussi, M., Palombo, M.R., (Eds.), Proceedings of the First International Congress, "The World of Elephants" Consiglio Nazionale delle Ricerche, Roma, pp. 305–309.

Rountrey, A.N., Fisher, D.C., Vartanyan, S., Fox, D.L., Carbon and Nitrogen Isotope Analyses of a Juvenile Woolly Mammoth Tusk: Evidence of Weaning. Quaternary International, this volume.

Rozanski, K., Araguás-Araguás, L., Gonfiantini, R., 1993. Isotopic patterns in modern global precipitation. In: Swart, P.K., Lohmann, K.C., McKenzie, J., Savin, S. (Eds.), Climate Change in Continental Isotopic Records. Geophysical Monograph 78. American Geophysical Union, Washington, DC, pp. 1–36.

Sher, A.V., Kuzmina, S.A., Kuznetsova, T.V., Sulerzhitsky, L.D., 2005. New insights into the Weichselian environment and climate of the East Siberian Arctic, derived from fossil insects, plants, and mammals. Quaternary Science Reviews 24, 533–569.

Stephan, E., 2000. Oxygen isotope analysis of animal bone phosphate: method refinement, influence of consolidants, and reconstruction of palaeotemperatures for Holocene sites. Journal of Archaeological Science 27, 523–535.

Sternberg, L.S.L., Mulkey, S.S., Wright, S.J., 1989. Oxygen isotope ratio stratification in a tropical moist forest. Oecologia 81, 51–56.

Stuart, A.J., 1991. Mammalian extinctions in the late Pleistocene of Northern Eurasia and North America. Biological Reviews 66, 453–562.

Stuart, A.J., 1999. Late Pleistocene megafaunal extinctions; a European perspective. In: MacPhee, R.D.E. (Ed.), Extinctions in Near Time: Causes, Contexts and Consequences. Kluwer Academic/Plenum Publishers, New York.

Stuart, A.J., 2005. The extinction of woolly mammoth (*Mammuthus primigenius*) and straight-tusked elephant (*Palaeoloxodon antiquus*) in Europe. Quaternary International 126–128, 171–177.

Vartanyan, S.L., Garutt, V.E., Sher, A.V., 1993. Holocene dwarf mammoths from Wrangel Island in the Siberian Arctic. Nature 362, 337–340.

Vartanyan, S.L., Arslanov, Kh.A., Tertychnaya, T.V., Chernov, S.B., 1995. Radiocarbon dating evidence for mammoths on Wrangel Island, Arctic Ocean, until 2000 BC. Radiocarbon 37, 1–6.

Whittington, S.L., Dyke, B., 1984. Simulating overkill: experiments with the Mosimann and Martin model. In: Martin, P.S., Klein, R.G. (Eds.), Quaternary Extinctions: A Prehistoric Revolution. University of Arizona Press, Tuscon, pp. 451–465.

Yakir, D., 1992. Variations in the natural abundance of oxygen-18 and deuterium in plant carbohydrates. Plant, Cell and Environment 15, 1005–1020.